Variability of marine 14C reservoir ages in the Southern Ocean highlighting circulation changes between 1910 and 1950

Martine Paterne, Elisabeth Michel, Virginie Héros

VARIABILITY OF MARINE ^{14}C RESERVOIR AGES IN THE SOUTHERN OCEAN HIGHLIGHTING CIRCULATION CHANGES BETWEEN 1910 AND 1950

Martine Paterne[1], Elisabeth Michel[1], Virginie Héros[2]

[1]Laboratoire des Sciences du Climat et de l'Environnement, LSCE/IPSL, CEA-CNRS-UVSQ, Université Paris-Saclay, Domaine du CNRS, F-91198 Gif-sur-Yvette

[2]Muséum d'Histoire Naturelle de Paris, Institut de Sytématique & Evolution, ISyEB (UMR 7205 CNRS/UPMC//MNHN/EPHE) 43 rue Cuvier 75231Paris France

Abstract

Recent changes in the Southern Ocean overturning circulation have been attributed either to natural variability or to anthropogenic forcing. The ^{14}C analyses of mollusk shells from Kerguelen Islands evidence a high decadal variability of the sea surface radiocarbon reservoir ages in the southern South Indian ranging from 832 to 1005 (±30) years between 1910 and 1930. Such high variability is common to the different sectors of the Southern Ocean, (southern South Pacific and Atlantic), at inter-annual and decadal timescales between 1901 and 1950. Notably, a decrease of $\Delta^{14}C$ of ~40‰ (increased R of ~290 years) occurred between 1901 and 1940, followed by an increase of ~30‰ between 1940 and 1958. Using a simple box model of ocean-atmosphere $^{14}CO_2$ exchange, this aging is attributed to increased upwelling of cold and ^{14}C-depleted subsurface seawaters due to intensified poleward Southern Westerlies. The sea surface ^{14}C aging is indeed well correlated to a positive phase of the Southern Hemisphere Annular Mode and to a cooling of the sea surface temperatures in the

Southern Ocean between 1901 and 1940. These pre-1950 sea surface ^{14}C changes highlight the importance of natural changes in wind intensities and ocean dynamics.

Keywords: Radiocarbon, Reservoir ages, Kerguelen *Is.*, Southern Westerlies- driven upwelling, Southern Ocean,

1. Introduction

The Southern Ocean (SO) is an important component of the global oceanic circulation with the redistribution of water masses between the Pacific, Atlantic and Indian Oceans by the Antarctic Circumpolar Current (ACC) (Fig. 1) (Tamsitt et al., 2017 *and references therein*). The strong westerlies in the Southern Hemisphere, combined with the Coriolis force, drive the ACC and a northward Ekman transport, permitting deep waters to upwell up to the surface at the Antarctic Divergence. In the last few decades, surface westerlies intensified poleward (Thompson & Solomon, 2002) that may give rise to significant changes in ocean circulation, carbon and heat uptake and biological productivity (Toggweiler & Samuels, 1995; Le Quéré et al., 2007; Sallée et al., 2010, 2012; Waugh et al., 2013; de Vries et al., 2017).

Significant changes of ocean ventilation in the Southern Ocean, such as the increase in the age of the circumpolar deep waters (CDW), were inferred from the analysis of chlorofluorocarbon-12 (CFC12) from early 1990s to 2000s and transport model simulations (Waugh et al., 2013). Similarly, using a global data assimilation ocean inverse model, and a carbon cycling model, DeVries et al. (2017) found an enhanced upper-ocean overturning circulation in 1990s relatively to 1980s and increased outgassing of natural CO_2. Both findings from analysis of CFC-12 and from inverse modeling are consistent with the expected increased northward Ekman drift and intensified upwelling resulting from westerlies intensification (Hall & Visbeck, 2002; Waugh et al., 2013; DeVries et al., 2017). Wind intensity is associated to a zonally symmetric structure in the atmospheric pressure gradient between the southern mid-latitudes and the polar regions of the SO, referred to as the Southern Annular Mode (SAM) (Thompson & Wallace, 2000; Thompson et al., 2000). In a positive phase the Westerlies, associated with higher than normal sea level pressures at the mid-latitudes and lower than normal at the high latitudes, are reinforced poleward, driving increased northward Ekman drift and intensified upwelling (Hall & Visbeck, 2002).

South of the Polar Front (PF), the sea surface reservoir ages (R), the difference between the marine and atmospheric ^{14}C ages at the same calendar age, are highly variable ranging from ~1000 to ~1500 years. They are based on the ^{14}C dating of solitary corals, mollusk shells, bones and flesh remains of penguins and seals of known ages, the ^{14}C of which representing that of the dissolved inorganic carbon (DIC) in seawater in which they grow. The values of R reflect the balance between the ^{14}C production and the ocean-atmosphere exchange of $^{14}CO_2$ as well as ocean dynamics (Stuiver et al., 1986) and their temporal variability reflect changes among these factors. Particularly, changes in zonal wind intensities in the Antarctic regions may significantly modify the ocean-atmosphere exchange and mixing between the sea surface and the ^{14}C-depleted underlying subsurface waters, and consequently the sea surface ^{14}C ages.

We present here new values of R estimated from mollusk shells collected between 1910 and 1930 off the Kerguelen *Is.* in the southern South Indian (SSI) where no values of R exist presently (Fig. 1). They are compared to previous estimates in the southwestern South Atlantic (SSA) (off Signy *Is.*) and in the southeastern South Pacific (SSP) (off the western Antarctic Peninsula and in the Ross Sea) in order to better understand the causes of the high variability of R in the Southern Ocean. We restricted our comparison to biogenic carbonates, though few, as penguins and seals remains may capture the ^{14}C content of different water masses due to the variety of diving depths, often very far from the Antarctic coasts (Biuw et al., 2007) (supplementary material, Table S1). After a brief description of the main hydrographic features at all the sample locations, the sea surface ^{14}C values are compared to those of DIC from early ^{14}C measurements of water samples before the nuclear bomb tests (Broecker et al., 1960; Rafter, 1972) and from the GLODAP reanalyses of the GEOSECS campaigns in the 70's (Rubin & Key, 2002; Key et al., 2004). They are further compared to the variations of the SAM index, based on the time series of the sea level pressure difference

between the Southern subtropical regions and Antarctica since 1860 (Marshall, 2003; Visbeck, 2009; Fogt et al., 2009; Jones et al., 2009) and to those of the annual sea surface temperature (SST) anomalies zonally averaged over the latitude bands 50°S-70°S, referred to as the Southern Ocean centennial variability (SOCV) index (Latif et al., 2013).

2 Material and methods

Mollusk shells, collected on Kerguelen *Is.*, were obtained from the collection of the Muséum National d'Histoire Naturelle de Paris (Fig. 1; supplementary material and Table S1). They are related to epifaunal species of gastropods, including two active predators *Neobuccinum eatoni* Smith (specimens from collections Rallier du Baty 1909 and Loranchet 1914) and one herbivore, *Nacella kerguelensis* Smith (collection Aubert de la Rue 1931). The date of collection corresponds to the year of sampling during scientific explorations on Kerguelen *Is.* by Rallier du Baty expedition in 1908/1909 and in 1913/1914, and by Aubert de la Rue in 1931. One epifaunal gastropod (1914) is still presenting tissues. The shells of the two other specimens are whole and intact, so they did not wear away before being collected, confirming that they were sampled alive.

Methods for radiocarbon analyses were described elsewhere (Tisnerat-Laborde et al., 2001). Chemical pre-treatment and carbonate hydrolyses were performed at the Gif-LSCE Radiocarbon Laboratory and graphite targets were prepared and measured at the French National AMS-ARTEMIS-LMC14 facility (Moreau et al., 2013). Results are expressed in conventional years BP (Table S1) and the $\Delta^{14}C$ ‰ is the deviation in parts per thousand (‰) of a sample's $^{14}C/^{12}C$ ratio corrected for year of growth from that of the absolute standard activity in 1950 (Stuiver and Polach, 1977). R is the difference between the measured ^{14}C age and the atmospheric ^{14}C age from the calibration record SHCal 13 in the southern Hemisphere

(Hogg et al., 2013), and ΔR the difference between the measured ^{14}C age and the modeled ocean one using the marine calibration dataset Marine13 (Reimer et al., 2013) at the date of the collection. Difference between previous published values and those presented in Table S1 are due to the different utilized calibration record.

3 Oceanographic setting

The Kerguelen plateau (water-depth <1000m) is a major topographic barrier where the eastward flowing ACC subdivides in two parts with the main flows associated to the Sub-Antarctic Front (SAF) and to the south by the Southern ACC front (SACCF) (Park et al., 2014) (Fig. 1). Between SAF and SACCF is located the polar front (PF), the path of which is observed either north or south of the Kerguelen *Is.* (Sokolov and Rintoul, 2009; Kim and Orsi, 2014; Park et al., 2014) and subject to large northward/southward shifts up to 100 km in a few tens of years (Sokolov and Rintoul, 2009; Kim and Orsi, 2014).

Deep waters from the southern Pacific, Atlantic and Indian Oceans enter the ACC within the Circumpolar Deep Water (CDW) (Orsi et al., 1993, 1995; Whitworth et al., 1994; Talley, 2013). From the South Atlantic, most of NADW, marked by high salinity in SO, enters the ACC, where it is modified by mixing with the locally formed deep waters of the lower core of CDW (LCDW). A small branch of NADW flows eastward directly into the South Indian upwelling as a component of the less dense deep Indian Water. The Indian and Pacific Deep Waters move southward to the ACC above NADW and form the upper core of CDW (UCDW), characterized by an O_2-minimum (Orsi et al., 1995; Talley, 2013). UCDW upwelling is balanced by a northward flow of low salinity that descends from the polar to the sub-Antarctic front (SAF) to form the Antarctic Intermediate Water characterized by a salinity

minimum. LCDW flows poleward and sinks along the continental slope mainly in the Weddell and Ross Seas and along Adélie Land as the Antarctic Bottom Water.

The Signy *Is.* are located in the vicinity of the Drake Passage on the Scotia Ridge where surface waters result from the mixing of the water bodies from the ACC and from the northwestern Weddell Sea (Whitworth et al., 1994) (Fig. 1). To the north of the shelf is located the southern front of the ACC where UCDW and LCDW upwell (Whitworth et al., 1994; Orsi et al., 1995). To the south, a branch of NADW penetrates CDW in the South Atlantic east of the Weddell Sea gyre near longitude 0°. Then it flows westward directly underneath the Antarctic surface water (AASW) and when reaching the Antarctic shelves it is transformed to the Weddell Sea Bottom Water Shelf waters (Whitworth et al., 1994; Orsi et al., 1995). From the South Atlantic, another branch of NADW flows eastward toward the Kerguelen Plateau (Orsi et al., 1993). Over the plateau and upstream Kerguelen *Is.*, AASW overlay the cold Winter Water (WW) at a water-depth of around 180-200 m (Park et al, 2008; Bowie et al., 2015). UCDW was observed below at 500m water-depth overlying LCDW (Bowie et al., 2015). Downstream, UCDW is observed at 600-800m water-depth with LCDW deeper than 1300m (Park et al, 2008; Quéroué et al., 2015). Over the southern Kerguelen plateau, UCDW is observed at depth of 400-1400m over LCDW (Park et al, 2008). On the western part of the Antarctic Peninsula, WW are observed at a water-depth of ~100m below the cold AASW (Orsi et al., 1995; Moffat et al., 2009). The UCDW intrudes the shelf as frequent and short events, but not as large-scale intrusions, while the 50-150m thick LCDW is inflowing to the shelf at depths of approximately 500m and below (Moffat et al., 2009).

All the considered samples of biogenic carbonates are located in the Antarctic surface waters within or south of the ACC (Fig. 1).

4 Results and Discussion

1) Values of R and •^{14}C off Kerguelen *Is.* and comparison with previous determinations of mollusk shells and seawater •^{14}C in the Southern Ocean

Values of R and $\Delta^{14}C$ of the biogenic carbonates ($\Delta^{14}C_{carb}$) off Kerguelen *Is.* range from 832 ± 31 years to 1005 ± 32 years and from -108.2 ± 3.2 to -131.9 ± 3.2 ‰, respectively, between 1909 and 1931 (Fig. 2; Table S1). Compared to these, greater R and more depleted $\Delta^{14}C_{carb}$ were measured from mollusk shells off the Antarctic Peninsula and from the eastern Ross Sea varying from 1088 ± 58 years to 1326 ± 40 years and from -136.9 ± 6 ‰ to -166.8 ± 3.9 ‰ respectively in the two regions. Values at Signy *Is.* are also greater than the measured ones off Kerguelen *Is.* at an average of 1109 ± 89 years and -146 ± 9.5 ‰. The statistical Chi-square tests indicate that, in each sector, the values of R and $\Delta^{14}C_{carb}$ are incompatible at the 95% confidence level attesting a highly significant variability of ^{14}C in the Antarctic surface water.

We compared the $\Delta^{14}C_{carb}$ to the natural $\Delta^{14}C_{DIC}$ estimated in their respective regions (Broecker et al., 1960; Rafter, 1972; Rubin & Key, 2002; Key et al., 2004) (Fig. 3; supplementary material, Table S2). Mean values of $\Delta^{14}C_{DIC}$ in UCDW and LCDW are calculated using the temperature, salinity and O_2 properties defined by Orsi et al. (1995). The sea surface and UCDW/LCDW values of $\Delta^{14}C_{DIC}$ are similar within the uncertainties in the southern South Pacific (SSP) along the Antarctic Peninsula and in the Ross Sea and they are not significantly different from those of Signy *Is.* in the southwestern South Atlantic (SSA). Values of $\Delta^{14}C_{DIC}$ in SSP and SSA are consequently grouped into a unique sector. The mean $\Delta^{14}C_{DIC}$ are lower in SSP-SSA than in SSI by ~20 ‰ for both the sea surface and UCDW/LCDW. In all the sectors, the values from mollusk shells mimic the high variability

of AASW $\Delta^{14}C_{DIC}$ and some are close or similar to those of UCDW and LCDW. This is also featured by the $\Delta^{14}C_{carb}$ of the corals from the Ross Sea ice shelves (Hall et al., 2010).

At Kerguelen *Is.*, the values of $\Delta^{14}C_{carb}$ linearly decrease with a highly significant regression coefficient (r^2=0.98) between 1909 and 1931 (Fig. 2). In the SSP-SSA sector, $\Delta^{14}C_{carb}$ significantly decrease linearly between 1917 and 1940 (r^2=0.76) while they do not vary between 1917 and 1953 (r^2=0.05), that is partly due to the high inter-annual variability of $\Delta^{14}C_{carb}$ of ~18‰ at Signy *Is.* at around 1950. This is also related to a well-marked reverse increasing trend in 1940 up to 1958 (r^2=0.73) considering the measured $\Delta^{14}C_{DIC}$ in 1958 in the southern South Atlantic, south of the ACC, and in the Ross Sea where the bomb-produced ^{14}C effect had a minimum impact (Broecker et al., 1960; Rafter, 1972) (Table S2). Between 1917 and 1940, the equation of the linear regression in SSP is very similar to that of SSI. Moreover, it is also similar and highly significant (r^2=0.87) when adding one value in 1901 from one coral from the Ross Sea (Hall et al., 2010) and when accounting for the calendar age uncertainty, which is greater than that of mollusk shells (supplementary material, Fig. S1). Finally, the negative trends of $\Delta^{14}C_{carb}$ in SSI and SSP between 1901 and 1940 have an offset of ~20 ± 7‰ that is very consistent with the estimated difference of $\Delta^{14}C_{DIC}$ between these sectors (Table S2). Subtracting 20‰ to the values of $\Delta^{14}C_{carb}$ at Kerguelen *Is.* results in a significant decrease of sea surface ^{14}C (r^2=0.90) between 1901 and 1940. We thus conclude that the observed decreases of $\Delta^{14}C_{carb}$ in the southern South Indian and South Pacific are robust statistical trends between 1901 and 1940 as well as the increase of $\Delta^{14}C_{carb}$ and between 1940 and 1958. The uncertainty of $\Delta^{14}C$, estimated from the square root of the variance, is ± 7-9‰ between 1901 and 1958 that is of the same order than the mean inter-annual changes of measured $\Delta^{14}C_{carb}$ at Signy *Is.*. In addition to the inter-annual variability, the record of $\Delta^{14}C$ from the biogenic carbonates and seawater DIC very likely reflects long-term changes of sea surface ^{14}C in the Southern Ocean, which are very likely due to common

processes acting on the global Southern Ocean sea surface ^{14}C. Using the values of the slopes and their uncertainties, the decrease of $\Delta^{14}C_{carb}$ would be of some ~10 ± 2‰ per decade between 1901 and 1940 and the sea surface $\Delta^{14}C$ increase per decade would be of some 18 ± 5 ‰ between 1940 and 1958.

2) Factors contributing to the variations of sea surface $\Delta^{14}C$ in the Southern Ocean

The inter-annual and decadal changes of sea surface $\Delta^{14}C$ in the Southern Ocean are much greater than the changes of ^{14}C in the atmosphere. Notably, the sea surface ^{14}C aging between 1900 and 1940 is 2 times greater than the contemporaneous aging of the atmosphere due to the industrial and domestic input of ^{14}C-depleted fossil fuels, known as the *Suess effect* (Hogg et al., 2013). Changes of the sea surface ^{14}C in the Southern Ocean can neither be attributed to changes in the extent of the sea-ice cover that inhibits the atmosphere-ocean $^{14}CO_2$ exchange, nor to changes in the outflow of old freshwaters from subglacial lake brines, such as in the Ross Sea (Mikucki et al., 2009), as such features do not exist at Kerguelen *Is.*.

Changes of the sea surface ^{14}C in the Southern Ocean may be the result of the variations of the flux of NADW into the CDW core waters as $\Delta^{14}C_{DIC}$ is higher in NADW at around -100‰ (Broecker et al., 1960) than in the southern South Indian and Pacific deep waters (Fig. 3). They may be also caused by changes of wind-induced mixing of sea surface with the cold and ^{14}C-depleted subsurface waters from UCDW or LCDW mediated by changes of either the mixed layer depth (MLD) or Ekman-induced upwelling. Nonetheless, the greatest wind-induced changes in MLD were observed within and north of the ACC rather than in the southernmost regions of the Southern Ocean (Sallée et al., 2010; Carranza and Gille, 2014).

We thus estimated the changes of R due to changes either in the NADW flux into the Southern Ocean or in upwelling intensities from simplified equations for a surface water box, exchanging with a deep box CDW and the atmosphere (supporting material, Fig. S2). The flux of NADW into CDW was changed by a factor of 2, as observed during the past 60 years for NADW intensity in the North Atlantic (Bryden et al., 2014; Atkinson et al., 2012). Augmenting the contribution of NADW from 40% (Ganachaud, 2003; Talley, 2013) to 57% decreases R in SO by 25 years, that is much lower than the measured decadal changes of ~80 years. Testing a 40% increase of the upwelling in SO, the sea surface ^{14}C ages were augmented by ~100 years. In our simple model, using a sinusoidal change in SO upwelling, the time lag of the maximum ^{14}C age response to changes in wind-driven upwelling fluxes is 6 years, but a coupled ocean-atmosphere model would better estimate the impact of winds on both the amplitude and timing of the oceanic changes of ^{14}C in SO. The 40% increase in upwelling at the Antarctic Divergence used in the test is of the same order of magnitude than that estimated by DeVries et al. (2017), using data assimilation of global oceanographic tracers (CFC, temperature and salinity) in the 1990s relative to 1980s in an inverse model of the upper ocean circulation. The impact of increased upwelling is clearly a robust candidate to account for the long-term sea surface changes of 80 years per decade in the SO.

We compared the temporal changes of $\Delta^{14}C$ against the 11 year - running mean filtered records of the SAM index (Visbeck, 2009) and of the SOCV index (Latif et al., 2013) (Fig. 4). After subtracting 20 ‰ from SSI $\Delta^{14}C_{carb}$ in order to normalize to SSP, the values of $\Delta^{14}C$ in the Southern Ocean were interpolated using a 3rd order polynomial fit between 1901 and 1958. The changes of $\Delta^{14}C$ in the Southern Ocean are significantly correlated with the variations of SAM (r^2=0.67) with a time lag of $\Delta^{14}C$ of 6 years and with those of SOCV (r^2=0.94) and a time lag of $\Delta^{14}C$ of 12years. Between 1901 and 1940, $\Delta^{14}C$ decreased when the wind strength increased and SST became colder and between 1940 and 1958 it increased

248 when the wind strength decreased and SST became warmer. The long-term changes of $\Delta^{14}C$
249 in the Southern Ocean are thus likely related to the changes of wind driven upwelling
250 intensities between 1900 and 1958. The poleward increase of westerlies between 1901 and
251 1940 led to increased upwelling similarly as determined from CFC analyses and inverse
252 modeling for the 1980s to the 2000s, when poleward Westerlies intensified (Waugh et al.,
253 2013; de Vries et al., 2017).

254 In the latitudinal bands 50°-70°S, the SST exhibit one cycle of centennial variability
255 (Latif et al., 2013) (Fig. 4B). Prior to 1901, few values of $\Delta^{14}C_{carb}$ exist from paired ^{14}C and
256 U/Th dating of corals from Ross Sea Ice Shelves (Hall et al., 2010). The two values of
257 $\Delta^{14}C_{carb}$ in 1847 and 1862 are compatible at -144.1± 8.4‰ and significantly more depleted
258 than that of the coral in 1901, indicating an increase of $\Delta^{14}C_{carb}$ prior to 1901 (supplementary
259 material). Between 1850 and 1958, the $\Delta^{14}C$ of corals, mollusks shells and seawater DIC from
260 the Ross Sea, Antarctic Peninsula and southern South Atlantic would vary along a potential
261 fluctuation of ~80—100 year, that should be examined more thoroughly.

262 The recent changes in wind intensities were attributed either to natural decadal
263 variability or to anthropogenic forcing due to increased greenhouse gases and ozone depletion
264 (Thompson and Solomon, 2002; Thompson et al., 2011) or both (Waugh et al, 2013; De Vries
265 et al., 2017). Between 1910 and 1940, wind intensities increase markedly such as between
266 1980 and 2000 (Visbeck, 2009), but the CO_2 input into the atmosphere increases moderately
267 by 10ppm (Rubino et al., 2013) while it augments by 45 ppm between 1980 and 2000
268 (Keeling 1976; Thoning et al., 1989). The changes of $\Delta^{14}C_{carb}$ in the Antarctic surface waters
269 that we linked to fluctuations in wind driven upwelling intensities provide further evidence of
270 the natural variability of the coupled ocean-atmosphere system at low frequency.

271

5 Conclusion

The ^{14}C analyses of mollusk shells collected on Kerguelen *Is.* evidence a high decadal variability of the sea surface radiocarbon reservoir ages in the southern South Indian ranging from 830 to 1005 (±30) years between 1909 and 1931. Such high variability of sea surface ^{14}C is common to the different sectors of the Southern Ocean at inter-annual and decadal timescales. In addition to inter-annual changes of $\Delta^{14}C_{carb}$ of 18‰ as observed in the southwestern South Atlantic, a noticeable sea surface decrease of ~40‰ (increased R of ~290 years) was evidenced between 1900 and 1940, followed by an increase of ~30‰ between 1940 and 1958. These pre-1950 variations are large compared to atmospheric variations and highlight the natural variability of the Southern Ocean reservoir ages.

Between 1900 and 1958, the temporal changes of sea surface ^{14}C in the Southern Ocean are well correlated to the indices of the wind strength and SST changes of SAM and SOCV, respectively. Aging of sea surface occurred when SAM changed to a positive phase and SST became colder between 1901 and 1940, and inversely later up to 1958. We suggest that wind driven upwelling of cold and ^{14}C-depleted waters up to the sea surface is the main factor controlling the observed changes in the sea surface ^{14}C content in the Southern Ocean.

Measurements of the past changes of sea surface ^{14}C from biogenic carbonates, such as those between 1840 and 1950, provide one way to approach the low frequency natural variability of the coupled ocean-atmosphere system. Further detailed ^{14}C analyses and model simulations would help in separating the natural and anthropogenic causes of the variability of the Southern Hemisphere Westerlies.

Acknowledgements

295 We are greatly indebted to MNHN for the loan of historical malacological material from
296 Kerguelen Archipelago. We thanked J.R. Toggweiler and an anonymous reviewer for their
297 useful comments. This work received the financial support of the CEA-CNRS-UVSQ and the
298 French/Swedish program from the Swedish Research Council (VR-349-2012-6278). Thanks
299 are due to E. Kaltnecker, C. Noury for technical support and the ARTEMIS-LMC14 team for
300 graphite targets preparation and AMS-^{14}C measurements.

301

References

Atkinson, C. P., Bryden, H. L., Cunningham, S. A. King, B. A., 2012. Atlantic transport variability at 25 N in six hydrographic sections. *Ocean Sci.*, 8, 497–523, doi:10.5194/os-8-497-2012.

Biuw, M., Boehme, L., Guinet, C., Hindell, M., Costa, D., Charrassin, J.-B., Roquet, F. Bailleul, F., Meredith, M., Thorpe, S., Tremblay, Y., McDonald, B., Park, Y. H., Rintoul, S. R., Bindoff, N., Goebel, M., Crocker, D., Lovell, P., Nicholson, J., Monks, F., Fedak, M. A., 2007. Variations in behavior and condition of a Southern Ocean top predator in relation to in situ oceanographic conditions. *Proc. Nat. Am. Sci.*, 104, 13705-13710.

Bowie, A. R., van der Merwe, P., Quéroué, F., Trull, T. , Fourquez, M., Planchon, F., Sarthou, G., Chever, F., Townsend, A. T., Obernosterer, I., Sallée, J.-B., Blain, S., 2015. Iron budgets for three distinct biogeochemical sites around the Kerguelen Archipelago (Southern Ocean) during the natural fertilisation study, KEOPS-2. *Biogeosci.*, 12, 4421–4445.

Broecker, W.S., Gerard, R., Ewing, M., Heezen, B.C. (1960. Natural Radiocarbon in the Atlantic Ocean. *J. Geophys. Res.*, 65, 2903-2931.

Bryden H. L., King B. A., McCarthy G. D., McDonagh, E. L., 2014. Impact of a 30 % reduction in Atlantic meridional overturning during 2009–2010. *Ocean Sci.*, 10, 683–691, doi:10.5194/os-10-683-2014.

Carranza, M. M., Gille, S. T., 2014, Southern Ocean wind-driven entrainment enhances satellite chlorophyll-a through the summer. *J. Geophys. Res.*, 120, 304–323, doi:10.1002/2014JC010203.

DeVries, T., Holzer, M., Primeau, F., 2017. Recent increase in oceanic carbon uptake driven by weaker upper-ocean overturning, *Nature*, 542, 214-219, doi :10.10138, nature21068.

Fogt, Ryan L.,Perlwitz, Judith, Monaghan, Andrew J. Bromwich, David H., Jones, Julie M., Marshall G.J., 2009. Historical SAM Variability. Part II: Twentieth-Century Variability and Trends from Reconstructions, Observations, and the IPCC AR4 Models. *J. Clim.*, 22, 5346-5365. Doi :10.1175/2009JCLI2786.1.

Ganachaud, A., 2003. Large-scale mass transports, water mass formation, and diffusivities estimated from World Ocean Circulation Experiment (WOCE) hydrographic data. *J. Geophys. Res.*, 108(C7), 3213, doi:10.1029/2002JC001565.

Hall, A., Visbeck, M., 2002. Synchronous Variability in the Southern Hemisphere Atmosphere, Sea Ice, and Ocean Resulting from the Annular Mode. *J. Clim.*, 15, 3043-3057.

Hall B. L., Henderson, G.M., Baroni C., Kellogg, T.B., 2010. Constant Holocene Southern-Ocean ^{14}C reservoir ages and ice-shelf flow rates. *Earth Plan. Sci. Lett.*, 296, 115-123.

Hogg, A.G., Hua, Q., Blackwell, P.G., Niu, M., Buck, C.E., Guilderson, T.P., Heaton, T.J., Palmer, J.G., Reimer, P.J., Reimer, R.W., Turney, C.S.M., Zimmerman, S.R.H., 2013. SHCal 13 Southern Hemisphere calibration, 0–50,000 years cal BP. *Radiocarbon*, 55(4), 1889–1903.

Jones, R. L., Fogt, M. Widmann, G. J. Marshall, P. D. Jones, Visbeck, M., 2009. Historical SAM variability. Part I: Century-length seasonal reconstructions. *J. Clim.*, 22, 5319–5345.

Keeling, C.D., Bacastow, R.B., Bainbridge, A.E., Ekdahl, C.A., Guenther, P.R., Waterman, L.S., 1976. Atmospheric carbon dioxide variations at Mauna Loa Observatory, Hawaii.

346 *Tellus*, 28, 538-551.

347 Key, R. M., Kozyr, A., Sabine, C. L., Lee, K., Wanninkhof, R., Bullister, J. L., Feely, R. A.,
348 Millero, F. J., Mordy, C., Peng, T.H., 2004. A global ocean carbon climatology: Results
349 from Global Data Analysis Project (GLODAP). *Global Biogeochem. Cycles*, 18, GB4031,
350 doi:10.1029/2004GB002247.

351 Kim, Y.S., Orsi, A.H., 2014. On the Variability of Antarctic Circumpolar Current Fronts
352 Inferred from 1992–2011 Altimetry. *J. Phys. Ocean.*, 44, 3054-3071, DOI: 10.1175/JPO-
353 D-13-0217.1.

354 Latif, M., Martin, T. Park, W., 2013. Southern Ocean Sector Centennial Climate Variability
355 and Recent Decadal Trends. *J. Clim.*, 26, 7767-7782.

356 Le Quéré, C., Rödenbeck, C., Buitenhuis, E. T., Conway, T.J., Langenfelds, R., Gomez, A.,
357 Labuschagne, C., Ramonet, M., Nakazawa, T., Metzl, N., Gillett, N., Heimann, M. , 2007.
358 Saturation of the Southern Ocean CO_2 Sink Due to Recent Climate Change. *Science*, 316,
359 1735-1738, doi :10.1126, science.1136188.

360 Marshall, G.J., 2003. Trends in the Southern Annular Mode from observations and reanalyses.
361 *J. of Clim.*, 16, 4134–4143.

362 Mikucki, J.A., Pearson, A., Johnston, D.T., Turchyn, A.V., Farquhar, J., Schrag, D.P., Anbar,
363 A.D., Priscu, J.C., Lee, P.A., 2009. A contemporary microbially maintained subglacial
364 Ferrous "Ocean". *Science*, 324, 397-400.

365 Moffat, C., Owens, B., Beardsley, R. C., 2009. On the characteristics of Circumpolar Deep
366 Water intrusions to the west Antarctic Peninsula Continental Shelf. *J. Geophys. Res.*, 114,
367 C05017, doi:10.1029/2008JC004955.

368 Moreau, C., Caffy, I., Comby, C., Delqué-Kolić, E., Dumoulin, J., Hain, S., Vincent, J. , 2013.
369 Research and Development of the Artemis ^{14}C AMS Facility: Status Report. *Radiocarbon*,
370 55(2), 331-337. doi:10.1017/S0033822200057441.

371 Orsi, A. H., Nowlin W. D. Jr, Whitworth, T., 1993. On the circulation and stratification of the
372 Weddell Gyre. *Deep-Sea Res.* I, 40. 169-203.

373 Orsi, A. H., Whitworth, T., Nowlin, W. D., 1995. On the meridional extent and fronts of the
374 Antarctic Circumpolar Current. *Deep-Sea Res.* I, 42, 641–673, doi:10.1016/ 0967-
375 0637(95)00021.

376 Park, Y.H., Roquet, F., Durand, I., Fuda, J. L., 2008. Large-scale circulation over and around
377 the Northern Kerguelen Plateau. *Deep Sea Res.*, Part II, 55, 566–581.

378 Park, Y-H., Durand, I., Kestenare, E., Rougier G., Zhou, M., d'Ovidio, F., Cotte, C., Lee, J.H.,
379 2014. Polar Front around the Kerguelen Islands: An up-to-date determination and
380 associated circulation of surface/subsurface waters. *J. Geophys. Res.*, 119, 6575–6592, doi:
381 10.1002/2014JC010061.

382 Quéroué, F., Sarthou, G., Planquette, H.F., Bucciarelli, E., Chever, F., van der Merwe, P.,
383 Lannuzel, D., Townsend, A.T., Cheize, M., Blain, S., d'Ovidio, F., Bowie, A. R., 2015.
384 High variability of dissolved iron concentrations in the vicinity of Kerguelen Island,
385 Southern Ocean). *Biogeosci. Discuss.*, 12, 231–270.

386 Rafter, T., 1972. Carbon-14 variations in Nature, Part 3 measurements in the south Pacific
387 and antarctic oceans. *New Zealand J. Sci.*, 11, 551-589.

388 Reimer, P.J., Bard, E., Bayliss, A., Beck, J.W., Blackwell, P.G., Bronk Ramsey, C., Buck,
389 C.E., Cheng, H., Edwards, R.L., Friedrich, M., Grootes, P.M., Guilderson, T.P., Haflidason,
390 H., Hajdas, I., Hatté, C., Heaton, T.J., Hoffmann, D.L., Hogg, A.G., Hughen, K.A., Kaiser,

391 K.F., Kromer, B., Manning, S.W., Niu, M., Reimer, R.W., Richards, D.A., Scott, E.M.,
392 Southon, J.R., Staff, R.A., Turney, C.S.M., van der Plicht, J., 2013. IntCal13 and Marine13
393 radiocarbon age calibration curves 0–50,000 years cal BP. *Radiocarbon*, 55(4), 1869–1887.

394 Rubin, S.I., Key, R.M., 2002. Separating natural and bomb produced radiocarbon in the
395 ocean: the potential alkalinity method. *Global Biogeoch. Cycles*, 16, 4, 1105,
396 doi:10.1029/2001GB001432

397 Rubino, M., Etheridge, D. M., Trudinger, C. M., Allison, C. E., Battle, M. O., Langenfelds, R.
398 L., Steele, L. P., Curran, M., Bender, M., White, J. W. C., Jenk, T.M., Blunier, T., Francey,
399 R.J., 2013). A revised 1000 year atmospheric $\delta^{13}C$ CO_2 record from Law Dome and
400 South Pole, Antarctica. *J. Geophys. Res. Atmosph.*, 118, 8482–8499,
401 doi:10.1002/jgrd.50668.

402 Sallée, J.B., Speer, K. G., Rintoul, S. R., 2010. Zonally asymmetric response of the Southern
403 Ocean mixed-layer depth to the Southern Annular Mode. *Nat. Geosci.*, 3, 273-
404 279DOI :10.1038/NGEO812.

405 Sallée, J.B., Matear, R.J., Rintoul, S.R., Lenton, A., 2012. Localized subduction of
406 anthropogenic carbon dioxide in the Southern Hemisphere oceans. *Nat. Geosci.*,
407 doi :10.1038/NGEO1523.

408 Schlitzer, R., Ocean Data View, https://odv.awi.de, 2018.

409 Sokolov, S., Rintoul, S. R., 2009. Circumpolar structure and distribution of the Antarctic
410 Circumpolar Current fronts: 2. Variability and relationship to sea surface height. *J.*
411 *Geophys. Res.*, 114, C11019, doi:10.1029/2008JC005248.

412 Stuiver, M., Polach, H.A., 1977. Discussion. Reporting of ^{14}C data. *Radiocarbon*, 19, 355-363.

413 Stuiver, M., Pearson, G.W., Braziunas, T.F., 1986. Radiocarbon age calibration of marine
414 samples back to 9000 cal yr BP. *Radiocarbon*, 28, 980-1021.

415 Talley, L.D.,, 2013. Closure of the global overturning circulation through the Indian, Pacific
416 and Southern Oceans: schematics and transports. *Oceanography*, 26, 80-97.

417 Tamsitt, V., Drake, H.F., Morrison, A.K., Talley, L.D., Dufour, C.O., Gray, A.R., Griffies,
418 S.M., Mazloff, M.R., Sarmiento, J.L., Wang, J., Weijer, W., 2017. Spiraling pathways of
419 global deep waters to the surface of the Southern Ocean. *Nat. Com.*, 8, 172, DOI:
420 10.1038/s41467-017-00197-0.

421 Thompson, D.W.J., Wallace, J.M., 2000. Annular mode in the extratropical circulation, Part I:
422 Month-to-month variability. *J. Clim.*, 13, 1000–1016.

423 Thompson, D.W.J., Solomon, S., 2002. Interpretation of recent Southern Hemisphere climate
424 change. *Science*, 296, 895–899.

425 Thompson, D.W.J., Wallace, J.M., Hegerl, G.C., 2000. Annular mode in the extratropical
426 circulation. Part II: Trends. *J. Clim.*, 13, 1018-1036.

427 Thompson, D.W.J., Solomon, S., Kushner, P.J., England, M.H., Grise, K.M., Karoly, D.J.,
428 2011. Signatures of the Antarctic ozone hole in Southern Hemisphere surface climate
429 change. *Nat. Geosci.*, doi :10.1038/NGEO1296.

430 Thoning, K.W., Tans, P.P., Komhyr, W.D., 1989. Atmospheric carbon dioxide at Mauna Loa
431 Observatory 2. Analysis of the NOAA GMCC data, 1974-1985. *J. Geophys. Res.*, 94,
432 8549-8565.

433 Tisnérat-Laborde, N., Poupeau, J.J., Tannau, J.F., Paterne, M., 2001. Development of a semi-

automated system for routine preparation of carbonate sample. *Radiocarbon*, 43 (2A), 299-304.

Toggweiler, J. R., Samuels, B., 1995. Effect of Drake Passage on the global thermohaline circulation. *Deep-Sea Res.* I, 42, 477–500.

Visbeck, M., 2009. A station-based southern annular mode index from 1884 to 2005. *J. Clim.*, 22, 940–950.

Waugh, D. W., Primeau, F., DeVries, T., Holzer, M., 2013. Recent Changes in the Ventilation of the Southern Oceans. *Science*, 339, 568-570.

Whitworth, T. III, Nowlin Jr, W. D., Orsi, A.H., Locarnini, R.A., Smith, S.G., 1994. Weddell Sea Shelf Water in the Bransfield Strait and Weddell-Scotia Confluence. *Deep-Sea Res.* I, 41, 629-641.

Figures Captions

Fig. 1: Map of the Southern Ocean from Ocean Data View (R. Schlitzer, 2018) with the location of mollusks shells (black stars), corals (white stars) and water samples stations from the GEOSECS campaigns (numbered circles) and from early cruises (lettered circles) in Broecker et al. (1960) (B) and Rafter (1972) (R). Hydrographic fronts are from Orsi et al. (1995): SAF: sub-Antarctic front; PF: polar front; SACC: Southern front of the ACC; Bdy: southernmost boundary of the ACC. The lower and higher values of R in the Southern South Indian (SSI), South Atlantic (SSA) and South Pacific (SSP) are also indicated (supplementary information in text section 1 and Table S1).

Figure 2: Radiocarbon ages (A), reservoir ages (B) and $\Delta^{14}C_{carb}$ (‰) (C) as a function of year A.D. of mollusk shells from Kerguelen *Is*. (squares), Antarctic Peninsula (black circles) and Ross Sea (grey circle), Signy *Is*. (triangles) (Table S2) and from Ross Sea corals (open circles) (Hall et al., 2010). Measured seawater $\Delta^{14}C_{DIC}$ in 1958 from the Ross Sea (dotted circles) (Rafter, 1972) and from the southern South Atlantic in the Weddell Sea (white triangle) (Broecker et al., 1960) are also shown on C. Between 1901 and 1940, linear regression equations and coefficients of correlation are shown for values of Kerguelen *Is*. (SSI); for shell values of the Antarctic Peninsula and Ross Sea (SSP1) and for shells and coral values of these two last regions (SSP2). Between 1940 and 1958, the linear regression equations and coefficients of correlation derive from values of $\Delta^{14}C_{carb}$ and seawater $\Delta^{14}C_{DIC}$ excluding the most ^{14}C-depleted value at -170‰ (supplementary material). Uncertainties on $\Delta^{14}C_{carb}$ (1σ) for SSI (grey lines), SSP1 (black lines) and SSP2 (dotted lines) are represented prior to 1940, as well as between 1940 and 1958 for SSP(3) (black lines) (see text).

Fig. 3: (A) Comparison of $\Delta^{14}C_{carb}$ and $\Delta^{14}C_{DIC}$ in SSI, SSA and SSP. Values of $\Delta^{14}C_{carb}$ and uncertainties (1σ) are reported for mollusk shells from Kerguelen *Is.* (SSI), Signy *Is.* (SSA), Antarctic Peninsula (AP) and Ross Sea (RS) (Table S2) and from corals in the Ross Sea (Hall et al., 2010) (SSP) with the same symbols than in Figure 2. Values of $\Delta^{14}C_{DIC}$ at the sea surface (plus), in UCDW (cross) and LCDW (double cross) are from early ^{14}C measurements of water samples before the nuclear bomb tests (B*: Broecker et al., 1960; R*: Rafter, 1972) and from GLODAP reanalyses of natural ^{14}C from stations (St) of the GEOSECS campaigns in the 70's (Rubin & Key, 2002; Key et al., 2004). The mean values of $\Delta^{14}C_{DIC}$ and standard deviations are underlined for sea surface (grey box) and UCDW-LCDW (dark grey box). Analytical errors and standard deviations of the means are reported at 1σ. Analytical errors of UCDW and LCDW, not drawn for graphic readability, range between 7 to 10 ‰ as an average (Broecker et al., 1960; Rafter, 1972; Rubin & Key, 2002; Key et al., 2004). Sea surface $\Delta^{14}C_{DIC}$ noted DP (Drake Passage) is from the northern edge of the ACC (supplementary material Table S2).

Fig. 4: Comparison of the changes of $\Delta^{14}C$ (same symbols than in Fig. 2) with the annual variations of SAM as a function of time (Year) (A). The dotted (annual) and dark grey (11yr running mean) records are from Visbeck (2009). Thin black line refers to records from Marshall (2003) and light grey line to Fogt et al. (2009) and Jones et al. (2009). Records are normalized for graphic convenience and correspond to 11yr-running means. (B) Same comparison with the annual (thin black) and 11yr running mean (bold grey) variations of SOCV (Latif et al., 2013). The thick black line in A and B represents a third order polynomial fit between the values of $\Delta^{14}C$, once subtracting 20‰ from the

494 $\Delta^{14}C$ from Kerguelen *Is.* (dotted squares) in order to normalize to SSP (see text). A
495 sinusoidal curve of a 100 yr period (dotted line) is also shown in (B).

496

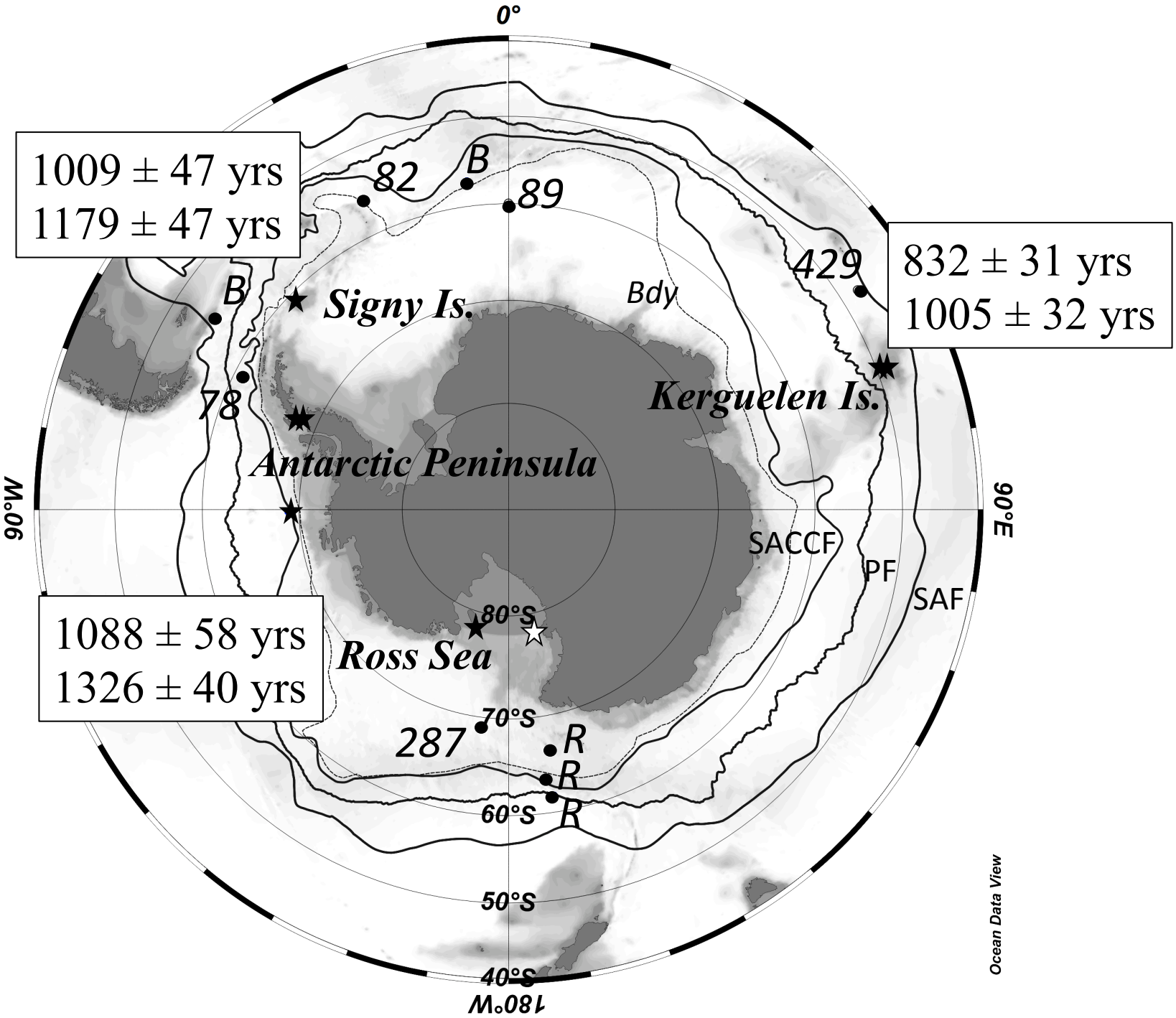
0°
90°W
90°E
180°W
1009 ± 47 yrs
1179 ± 47 yrs
832 ± 31 yrs
1005 ± 32 yrs
1088 ± 58 yrs
1326 ± 40 yrs
82
B
89
429
B
78
287
R
R
R
Signy Is.
Bdy
Kerguelen Is.
Antarctic Peninsula
Ross Sea
SACCF
PF
SAF
80°S
70°S
60°S
50°S
40°S
Ocean Data View

Figure 1

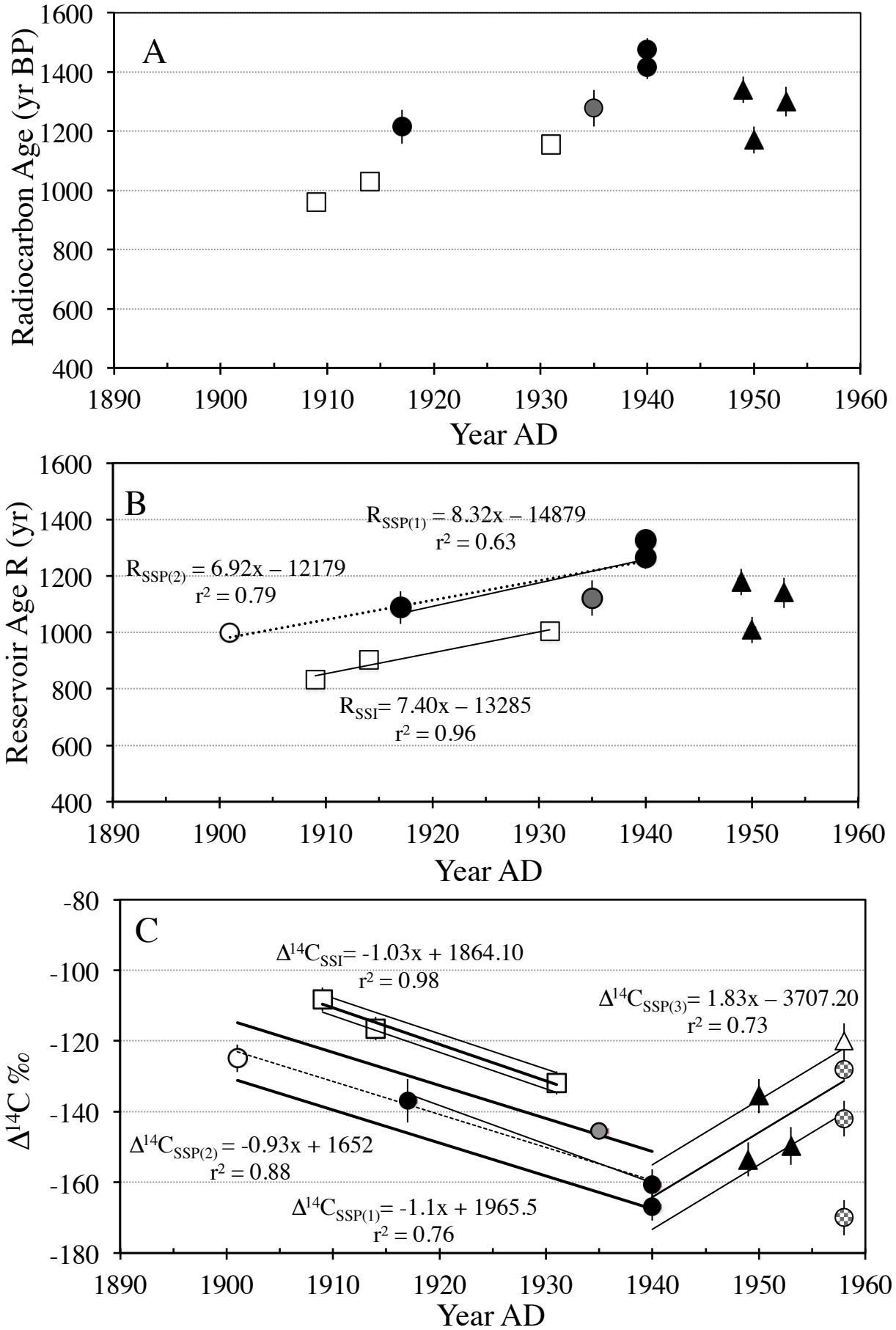
A
Radiocarbon Age (yr BP)
1600
1400
1200
1000
800
600
400
1890
1900
1910
1920
1930
1940
1950
1960
Year AD
B
Reservoir Age R (yr)
$R_{SSP(1)}$ = 8.32x – 14879
r^2 = 0.63
$R_{SSP(2)}$ = 6.92x – 12179
r^2 = 0.79
R_{SSI}= 7.40x – 13285
r^2 = 0.96
Year AD
C
$\Delta^{14}C$ ‰
$\Delta^{14}C_{SSI}$= -1.03x + 1864.10
r^2 = 0.98
$\Delta^{14}C_{SSP(3)}$= 1.83x – 3707.20
r^2 = 0.73
$\Delta^{14}C_{SSP(2)}$ = -0.93x + 1652
r^2 = 0.88
$\Delta^{14}C_{SSP(1)}$= -1.1x + 1965.5
r^2 = 0.76
-80
-100
-120
-140
-160
-180
Year AD

Fig 2

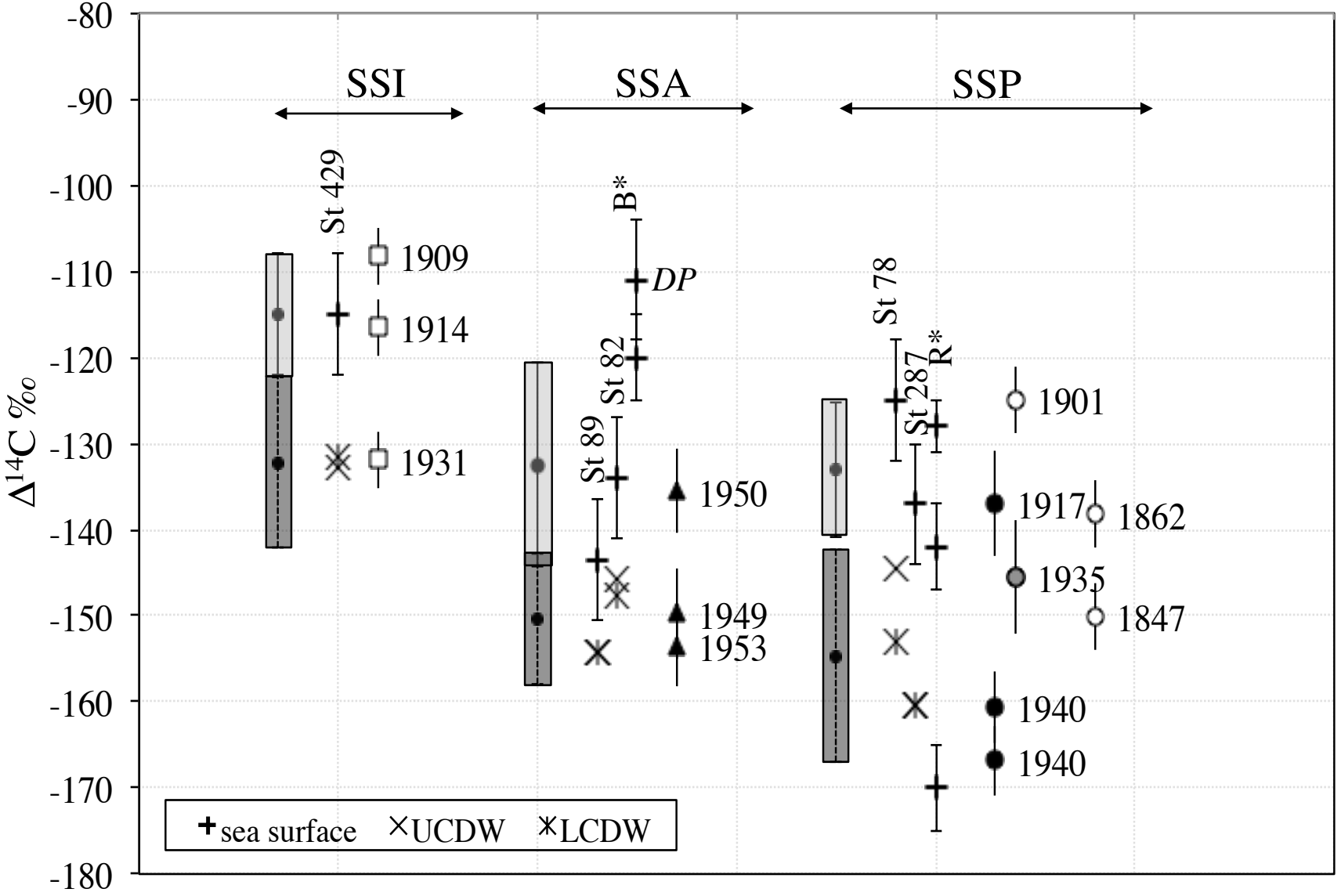
-80
-90
-100
-110
-120
-130
-140
-150
-160
-170
-180
Δ14C ‰
SSI
SSA
SSP
St 429
1909
1914
1931
B*
DP
St 82
St 89
1950
1949
1953
St 78
St 287
R*
1901
1917
1862
1935
1847
1940
1940
sea surface
UCDW
LCDW

Fig. 3

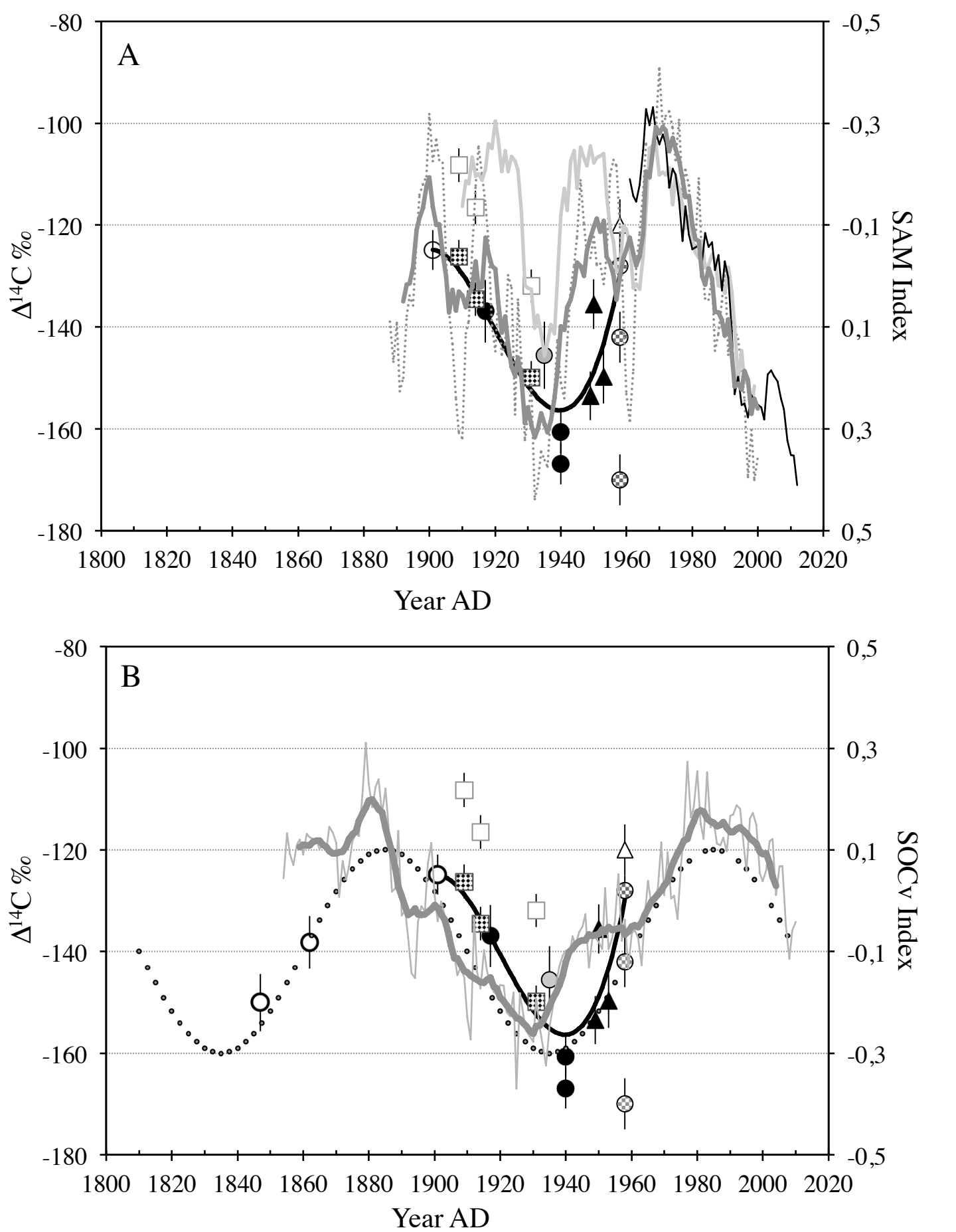
A
-80
-100
-120
-140
-160
-180
-0,5
-0,3
-0,1
0,1
0,3
0,5
Δ14C ‰
SAM Index
1800 1820 1840 1860 1880 1900 1920 1940 1960 1980 2000 2020
Year AD
B
-80
-100
-120
-140
-160
-180
0,5
0,3
0,1
-0,1
-0,3
-0,5
Δ14C ‰
SOCv Index
1800 1820 1840 1860 1880 1900 1920 1940 1960 1980 2000 2020
Year AD

Fig. 4